



## Radial Permeability Measurements for Shale Using Variable Pressure Gradients

FAN Kunkun<sup>1,2,3,\*</sup>, SUN Renyuan<sup>3</sup>, Derek ELSWORTH<sup>4</sup>, DONG Mingzhe<sup>3,5</sup>,  
LI Yajun<sup>3</sup>, YIN Congbin<sup>6</sup>, LI Yanchao<sup>6</sup>, CHEN Zhongwei<sup>7</sup> and WANG Chunguang<sup>1,2</sup>

<sup>1</sup>State Key Laboratory of Mining Disaster Prevention and Control, Shandong University of Science and Technology, Qingdao 266555, China

<sup>2</sup>College of Energy and Mining Engineering, Shandong University of Science and Technology, Qingdao 266555, China

<sup>3</sup>College of Petroleum Engineering, Chinese University of Petroleum, Qingdao 266555, Shandong, China

<sup>4</sup>Energy and Mineral Engineering, Pennsylvania State University, PA 16801, USA

<sup>5</sup>Department of Chemical and Petroleum Engineering, University of Calgary, AB T2N1N4, Canada

<sup>6</sup>Downhole Service Company, Chuanqing Drilling Company, CNPC, Chengdu 610051, Sichuan, China

<sup>7</sup>School of Mechanical and Mining Engineering, The University of Queensland, QLD 4074, Australia

**Abstract:** Shale gas is becoming an important component of the global energy supply, with permeability a critical controlling factor for long-term gas production. Obvious deviation may exist between helium permeability determined using small pressure gradient (SPG) methods and methane permeability obtained under actual field production with variable pressure gradients (VPG). In order to more accurately evaluate the matrix permeability of shale, a VPG method using real gas (rather than He) is established to render permeability measurements that are more representative of reservoir conditions and hence response. Dynamic methane production experiments were performed to measure permeability using the annular space in the shale cores. For each production stage, boundary pressure is maintained at a constant and the gas production with time is measured on the basis of volume change history in the measuring pump. A mathematical model explicitly accommodating gas desorption uses pseudo-pressure and pseudo-time to accommodate the effects of variations in pressure-dependent PVT parameters. Analytical and semi-analytical solutions to the model are obtained and discussed. These provide a convenient approach to estimate radial permeability in the core by nonlinear fitting to match the semi-analytical solution with the recorded gas production data. Results indicate that the radial permeability of the shale determined using methane is in the range of  $1 \times 10^{-6}$ – $1 \times 10^{-5}$  mD and decreases with a decrease in average pore pressure. This is contrary to the observed change in permeability estimated using helium. Bedding geometry has a significant influence on shale permeability with permeability in parallel bedding orientation larger than that in perpendicular bedding orientation. The superiority of the VPG method is confirmed by comparing permeability test results obtained from both VPG and SPG methods. Although several assumptions are used, the results obtained from the VPG method with reservoir gas are much closer to reality and may be directly used for actual gas production evaluation and prediction, through accommodating realistic pressure dependent impacts.

**Key words:** shale, radial permeability, variable pressure gradients, pseudo pressure, pseudo time

Citation: Fan et al., 2020. Radial Permeability Measurements for Shale Using Variable Pressure Gradients. Acta Geologica Sinica (English Edition), 94(2): 269–279. DOI: 10.1111/1755-6724.14304

### 1 Introduction

Commercial production of shale gas is achieved through modern developments in horizontal drilling and multi-stage hydraulic fracturing (Lin, 2016; Fan et al., 2018a; Guo et al., 2018; Parvizi et al., 2018; Shan et al., 2018). Although fracture properties may dominate the levels of gas production in the early stages of recovery, it is the permeability of the shale matrix that controls the performance of gas wells over the long-term (Heller et al., 2014; Cicha-Szot et al., 2015). Previous studies (Knabe and Wang, 2011; Heller et al., 2014; Guo et al., 2015; Cui and Abass, 2016; Wang et al., 2016a) often estimate shale

permeability through investigating gas flow characteristics along the axial direction of the core. However, both linear and radial flow regimes occur simultaneously in fractured shale formations (Ozkan et al., 2010; Cicha-Szot et al., 2015; Liu, 2016; Wang et al., 2017a; Wang et al., 2017b). Thus, determining the radial matrix permeability is of great importance to understand seepage mechanisms and the likely shale gas production performance.

Permeability measurement methods can be divided into two categories based on the evaluation approach: indirect and direct methods. In the indirect method, the apparent matrix permeability is determined by establishing a mathematical model on the basis of the pore size distribution (PSD) (Tian et al., 2017). The PSD can be determined experimentally by mercury injection (Brown,

\* Corresponding author. E-mail: fankunkun06@qq.com.

2015), polarization decay (Tong et al., 2006; Revil and Florsch, 2010) and nuclear magnetic resonance (NMR) (Daigle and Dugan, 2011). The model is derived from theoretical aspects of gas-molecule interactions with the pore walls, potentially accounting for unique flow behaviors involving viscous flow, slip flow and Knudsen diffusion (Javadpour et al., 2007; Javadpour, 2009; Freeman et al., 2011; Okamoto et al., 2015; Tian et al., 2017; Song et al., 2018). Although accommodating these flow regimes in the model, this method must be validated against experimental or field production data. When applying the direct method, permeability is measured by either steady state (through the application of a constant pressure gradient or gas flow rate) (API, 1998), or unsteady state techniques (analysis of the change in pressure gradient or fractional gas production as a function of time) (Brace et al., 1968; Bourbie and Walls, 1982; Suarez-Rivera et al., 2012; Qu et al., 2015; Yang et al., 2015). The former is time consuming for ultralow permeability measurements (Sinha et al., 2012), and the latter requires a transient flow model corresponding to the experimental measurements as well as a reliable method to appraise the permeability model parameters (Cui et al., 2009; Yang et al., 2015; Ettehadtavakkol and Jamali, 2016).

Among these methods mentioned above, the unsteady technique is the most suitable method for shale permeability measurement because it can both reduce the duration of individual experiments and increase the robustness of the estimation (Ettehadtavakkol and Jamali, 2016). This method has been fully developed and extensively used (Jones, 1972; Hsieh et al., 1981; Neuzil et al., 1981; Bourbie and Walls, 1982; Luffel et al., 1993; Jones, 1997; Haskett et al., 1998; Cui et al., 2009; Yang et al., 2015; Cui and Abass, 2016; Ettehadtavakkol and Jamali, 2016). However, current unsteady techniques are established on the basis of a small pressure gradient (SPG) and simplify the mathematical model by assuming constant PVT properties of the gas. This approximation is not consistent with gas production under reservoir conditions with variable pressure gradients (VPG) and may lead to erroneous results, due to pressure-dependent gas properties (Al-Hussainy et al., 1966; Zhang and Ayala, 2015). Therefore, a VPG technique is essential for the reliable and accurate determination of shale permeability.

The following presents a method to determine permeability under conditions of variable pressure gradients. First, dynamic production experiments under a constant external pressure are conducted to measure methane dynamic production characteristics with three designated pressure gradients. Then, a mathematical model explicitly accommodating gas variable PVT parameters and desorption for radial flow in individual shale cores is established. A workflow for the estimation of radial permeability via a VPG method is presented. Finally, the quality of the resulting predictions is discussed, together with the identification of some limitations of the method.

## 2 Geological Settings

The Sichuan Basin is an area of approximately  $1.8 \times 10^5$

km<sup>2</sup> in Southwest China, surrounded by several mountains, e.g. Micang Mountain, Dalou Mountain and Longmen Mountain (Chen et al., 2011; Chen et al., 2018; Fan et al., 2019; Huang et al., 2019), as shown in Fig. 1. This basin is a prolific hydrocarbon region and is estimated to have  $0.44 \times 10^9$  m<sup>3</sup> of exploitable shale gas resources, offering the most potential for shale gas development of any area in China (Yu et al., 2016; Wu et al., 2017). Several different intervals of source rocks, from the Cambrian and the Silurian through the Permian and the Triassic to the Jurassic, contribute to the total quantity of gas in place (Chen et al., 2011). Amongst these intervals, the Longmaxi Formation formed at the Early Silurian is the most widespread, with a thickness larger than 200 m. This formation is organic-rich with a total organic content (TOC) ranging from 0.45% to 8.75% (Luo et al., 2012), and is overmature as indicated by a  $R_o$  larger than 2% (Chen et al., 2011). Both shallow and deep shelf facies are present, according to the depositional environments. The shallow shelf sediments are dominated by siltstone, while the deep shelf sediments contain silty shales, dark gray mudstones, laminar muddy siltstones and siltstones. The dark organic-rich shales generally represent the 'sweet spot' for gas accumulation and storage (Guo et al., 2014; Nei and Jin 2016; Zhao et al., 2016).

## 3 Experiment and Theory

We conducted dynamic methane production tests to estimate the radial permeability and desorption potential of shale cores. In order to accommodate variations on pressure-dependent PVT parameters, pseudo-pressure and pseudo-time were used to perform the analysis via mathematical modeling.

### 3.1 Methane dynamic production experiments

Experiments were performed on shale samples collected from the Fuling shale play, southeast of Chongqing, Sichuan, China. This field is a deep water shelf marine shale with natural bedding fractures (Guo et al., 2014b; Ou and Li, 2017). Two cores were prepared from the Longmaxi Formation by drilling both parallel and perpendicular to the bedding orientation. Table 1 summarizes the petrophysical properties of the shale.

Figure 2 shows a schematic diagram of the dynamic methane production apparatus. The shale core is inserted vertically in the sample chamber with its two ends sealed by epoxy resin. This prevents flow from the top and bottom of the core and allows a fully radial flow regime. The intermediate chamber is connected to the measuring pump. The temperature-controlled system contains a thermostat and a water bath (accuracy of 0.01°C). This design guarantees constant temperature conditions for the gas production experiments.

Before conducting the dynamic production test, both volume correction and leakage tests were conducted for the entire system using helium. Then, the entire system was placed under vacuum for at least 12 h, until the system pressure reached  $10^{-3}$  Pa. The core sample was pressurized to 10 MPa for more than 1 day to obtain a uniform gas pressure distribution in the core. Gas

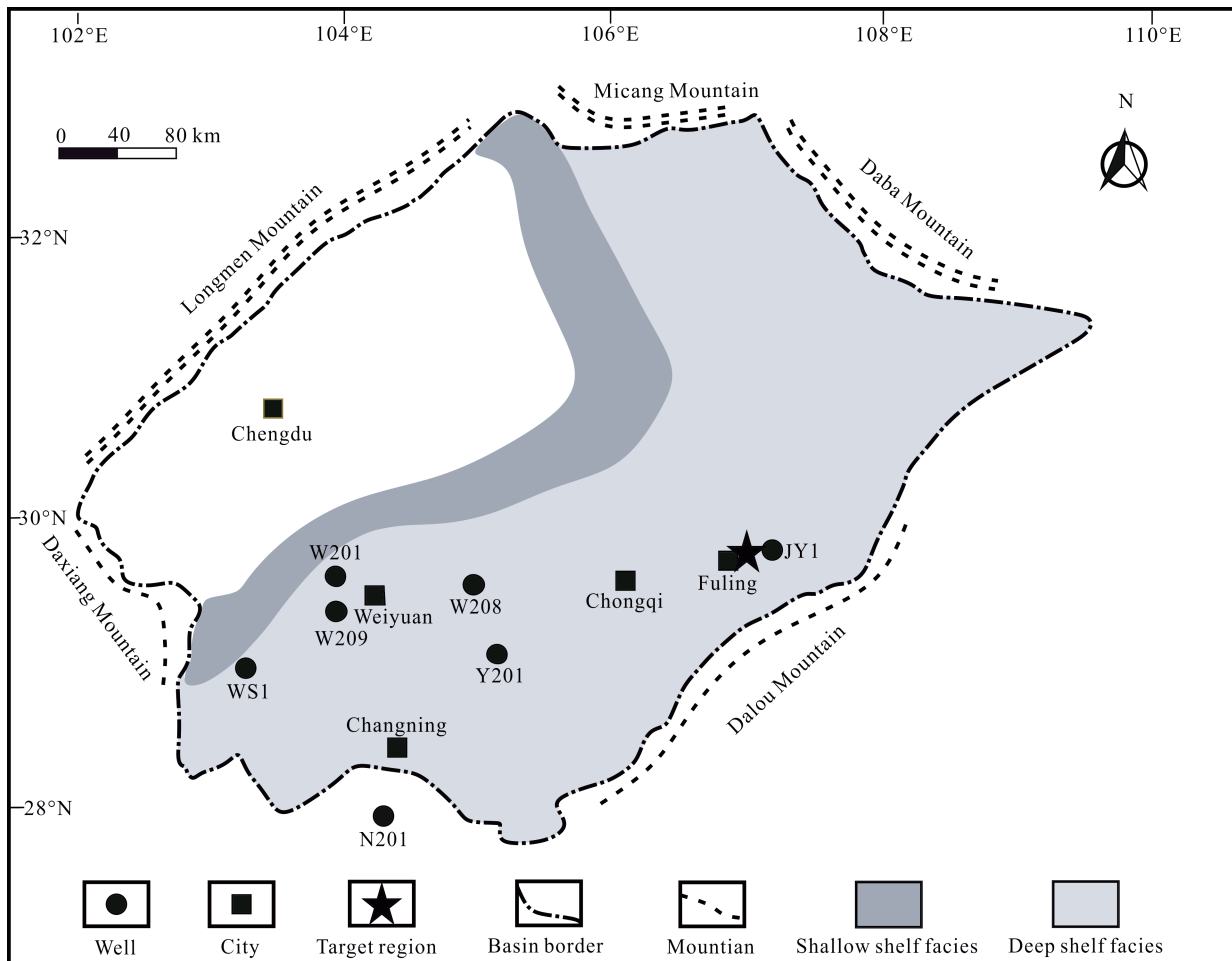


Fig. 1. Distribution of sedimentary facies of the Longmaxi shale in the Sichuan Basin (modified after Chen et al., 2011; Guo et al., 2014; and Ran et al., 2016).

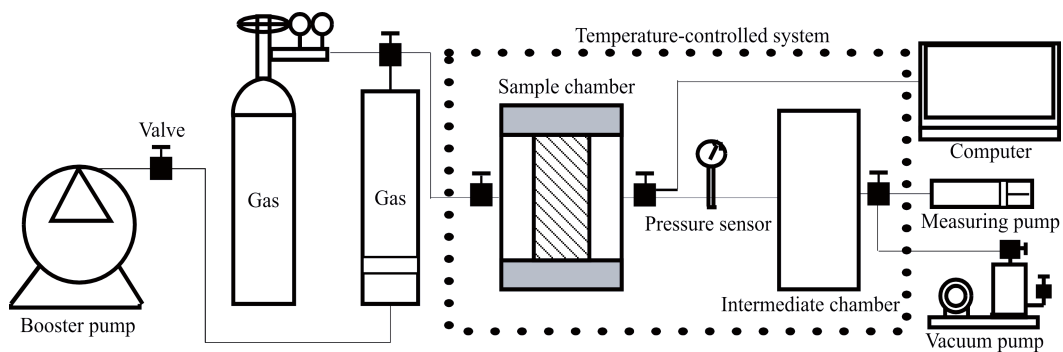


Fig. 2. Schematic diagram of the experimental apparatus.

**Table 1 Petrophysical characteristics of the shale**

Sample	Length (cm)	Porosity (%)	Skeleton density (cm <sup>3</sup> /g)	TOC (wt %)	Clay content (wt %)
1	3.25	4.52	2.83	2.81	18.28
2	4.55	4.49			

production tests were conducted in stepped-pressure production stages with three designated pressure decrements of approximately 10 MPa to 6 MPa, 6 MPa to 2 MPa and 2 MPa to 0.14 MPa. For each stage, the production pressure was maintained at a constant by

adjusting the measuring pump (Wang et al., 2016c; Yang et al., 2016). The accumulative gas production-time curve was evaluated by recording the volume change in the measuring pump with time. All experiments were conducted at a temperature of 35°C.

### 3.2 Evaluation methodology

The radial permeability of the shale is calculated by matching the semi-analytical solution of the radial flow model with the dynamic gas production data. Here, the methodology is introduced step-by-step.

### 3.2.1 Conceptual model

The sealed upper and lower end faces allow for strictly one-dimensional radial flow, as illustrated in Fig. 3. During a given dynamic production stage, the pressure drop migrates from the exterior to the interior of the shale pores until an equilibrium uniform pressure is attained that is equivalent to the initial external pressure. Both free gas and desorbed gas transport evolves with the VPG model accommodating both processes.

A dimensionless desorption coefficient is adopted to scale the gas desorption behaviors, defined as the ratio of the rate of change for the adsorbed gas density to that for the density of the free gas. In order to simplify the solution of the model, some reasonable assumptions were used as below:

(1) Petrophysical properties of the cylindrical core are homogeneous, e.g. pore structure, desorption rate coefficient and permeability.

(2) Single phase radial flow of gas progresses at a constant temperature and boundary pressure in cylindrical pores (e.g. Fig. 3). Gas permeability is constant at each production stage.

(3) The gas adsorption/desorption isotherm is described by a Langmuir equation. Thus, the desorption coefficient can be written as (Cui et al., 2009):

$$k_{ads} = \frac{\rho_s}{V_{std}} \cdot \frac{\partial \left( \frac{V_L P}{P_L + P} \right) / \partial t}{\partial \rho / \partial t} \quad (1)$$

where  $\rho_s$  is the skeletal density of the shale,  $V_{std}$  is the standard molar volume of gas (at 273.15 K and 0.101325 MPa),  $V_L$  is the Langmuir volume,  $P_L$  is the Langmuir pressure,  $P$  is pressure, and  $\rho$  is the volume density of free gas.

To verify the rationale for this simplification, each assumption is discussed below. The first approximation strategy (#1) has been widely used to establish gas flow models during production analysis (Cui et al., 2009; Yuan et al., 2014; Ettehadtavakkol and Jamali, 2016; Yang et al., 2016; Yang and Dong, 2017). The temperature and boundary pressure (assumption #2) are controlled to remain constant in the experiment by using a water bath and measuring pump, respectively. Thus, their fluctuation is controllably small. Using constant permeability within a certain pressure drop range is also acceptable, as has been verified and widely used in the

measurements of gas permeability in tight reservoirs (Suarez-Rivera et al., 2012; Qu et al., 2015; Cui and Abass, 2016). Finally, the Langmuir equation (assumption #3) is both well-known and broadly applied (Ross and Bustin, 2007; Bustin et al., 2008; Fan et al., 2017; Guo et al., 2017).

### 3.2.2 Mathematical model

With the above assumptions, the governing equation describing the radial flow can be written as:

$$\phi_e \frac{\partial \rho}{\partial t} + (1 - \phi_e) k_{ads} \frac{\partial \rho}{\partial t} = \frac{K}{r} \frac{\partial}{\partial r} \left( r \frac{1}{\mu c_g} \frac{\partial \rho}{\partial r} \right) \quad (2-1)$$

with initial and boundary conditions:

$$\rho \Big|_{0 \leq r < R, t=0} = \rho_i \quad (2-2)$$

$$\rho \Big|_{r=R, t \geq 0} = \rho_0 \quad (2-3)$$

$$\frac{\partial \rho}{\partial r} \Big|_{r=0} = 0 \quad (2-4)$$

where  $\phi_e$  is the effective porosity (Cui et al., 2009),  $k$  is the matrix permeability,  $\mu$  is gas viscosity,  $r$  is the distance between the center of the radial model and the point of interest,  $t$  is time and  $c_g$  is gas compressibility, defined as:

$$c_g = \frac{1}{P} - \frac{1}{Z} \frac{dZ}{dP}$$

In the SPG method, the governing equation is solved under the assumption that the gas PVT parameters remain constant over a small pressure drop (Cui et al., 2009; Cui and Abass, 2016; Yang and Dong, 2017). However, this hypothesis is inappropriate when measurements are conducted over a broad range of pressures. In the VPG model, we adopt pseudo-pressure and pseudo-time to account for the change of gas PVT properties and simplify the solution.

The pseudo-pressure is formulated as (Al-Hussainy et al., 1966):

$$m(P) = 2 \int_{P_i}^P \frac{P}{\mu Z} dP \quad (3)$$

where  $P_i$  is the pressure of the lower limit of integration.

After some rigorous transformations, Eq. (3) is followed by:

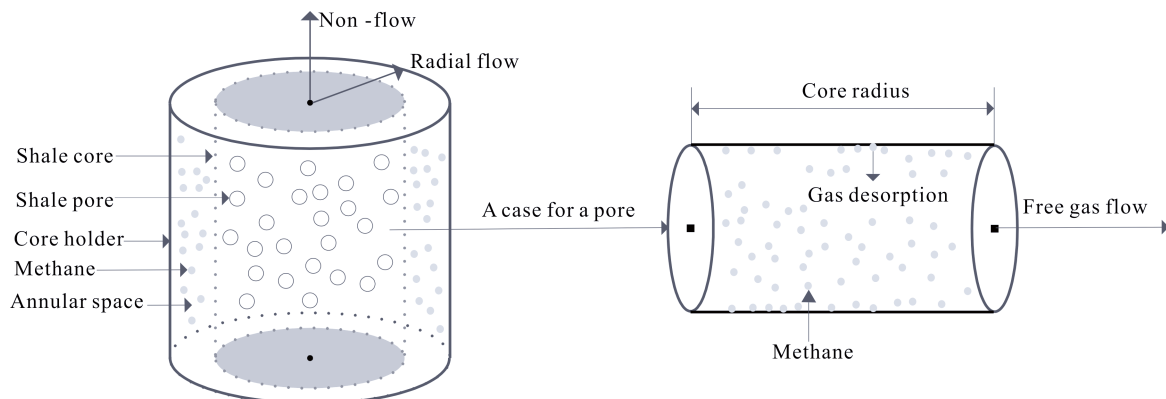


Fig. 3. Conceptual model of gas flow from shale core in the radial direction from interior to exterior.

$$\frac{\partial m(P)}{\partial t} = \frac{\partial m(P)}{\partial p} \cdot \frac{\partial P}{\partial t} = \frac{2P}{\mu Z} \cdot \frac{\partial P}{\partial t} \quad (4)$$

and

$$\frac{\partial m(P)}{\partial r} = \frac{2P}{\mu Z} \cdot \frac{\partial P}{\partial r} \quad (5)$$

The pseudo-time is defined as (Agarwal, 1979; Rahman et al., 2004):

$$m(t) = \int_0^t \frac{\mu_i c_{gi}}{\mu(\bar{P}) c_g(\bar{P})} dt \quad (6)$$

where  $\mu(\bar{P})$  and  $c_g(\bar{P})$  are the gas viscosity and compressibility respectively at average pressure  $\bar{P}$ .

The average pressure can be calculated by using the material balance equation:

$$Q_i - \frac{V_L \bar{P}}{P + P_L} - V_p \frac{\bar{P} Z_{sc} T}{P_{sc} Z T} = Q(t) \quad (7)$$

where  $Q_i$  is the total amount of gas in shale samples at initial conditions,  $V_p$  is the pore volume per unit weight,  $Q(t)$  is the amount of gas production at actual time  $t$ , and  $Z_{sc}$  and  $\bar{Z}$  are the gas compressibility factors at standard and average pressure, respectively.

The derivative of Eq. (6) with respect to time shows that:

$$\frac{\partial m(P)}{\partial t} = \frac{\partial m(P)}{\partial m(t)} \cdot \frac{\partial m(t)}{\partial t} = \frac{1}{\mu(\bar{P}) c_g(\bar{P})} \cdot \frac{\partial m(P)}{\partial m(t)} \quad (8)$$

Substituting Eq. (4), Eq. (5) and Eq. (8) into Eq. (2) with the product  $\mu c_a$  approximated at the average pressure, we obtain:

$$\frac{\partial m(P)}{\partial m(t)} = T_0 \frac{1}{r} \frac{\partial}{\partial r} \left( r \frac{\partial m(P)}{\partial r} \right) \quad (9-1)$$

$$m(P) \Big|_{0 \leq r < R_a, t=0} = m_i \quad (9-2)$$

$$m(P) \Big|_{r=R_a, t \geq 0} = m_0 \quad (9-3)$$

$$\left. \frac{\partial m(P)}{\partial r} \right|_{r=0} = 0 \quad (9-4)$$

where

$$T_0 = \frac{K}{\mu_i c_{gi} (\phi_e + (1 - \phi_e) k_{ads})} \quad (10)$$

Eq. (8) is a linearized diffusivity equation for real gas flow and its analytical solution can be obtained by a Laplace transform (Crank, 1975; Yang and Dong, 2017), given as:

$$m(P) = m(P_0) - \frac{2m(P_0)}{R_a} \sum_{n=1}^{\infty} \frac{J_0(r \xi_n) e^{-T_0 \xi_n^2 m(t)}}{\xi_n J_1(R_a \xi_n)} \quad (11)$$

where  $J_0(x)$  is the Bessel function of the first kind of order zero,  $J_1(x)$  is the Bessel function of the first order, and  $\xi_n$  is the positive root of equation  $J_0(R_a \xi_n) = 0$ .

### 3.2.3 Permeability determination

We define fractional gas production,  $F_D$ , as the ratio of the cumulative gas production at time  $t$  to the ultimate cumulative production. The gas production capacity can be written as:

$$\Omega(P) = Q_i - \left[ (1 - \phi_e) \frac{V_L P}{P + P_L} + \phi_e \frac{P}{ZRT} \right] \quad (12)$$

with  $Q_i$  written as:

$$Q_i = \left( (1 - \phi_e) \frac{V_L P_i}{P_0 + P_L} + \phi_e \frac{P_i}{ZRT} \right) \quad (13)$$

Thus  $F_D$  can be formulated as:

$$F_D = \frac{\Omega(P)}{\Omega(P_0)} = \frac{(1 - \phi_e) \frac{V_L P_i}{P_i + P_L} + \phi_e \frac{P_i}{ZRT} - (1 - \phi_e) \frac{V_L P}{P + P_L} - \phi_e \frac{P}{ZRT}}{(1 - \phi_e) \frac{V_L P_i}{P_i + P_L} - \phi_e \frac{P_i}{ZRT} - (1 - \phi_e) \frac{V_L P_0}{P_0 + P_L} + \phi_e \frac{P_0}{ZRT}} \quad (14)$$

Where  $P_0$  is the external pressure.

Previous studies indicate that a linear relationship between pseudo-pressure  $m(P)$  and pressure  $P$  appears during the primary half stage of the pressure drop (Etehadtavakkol and Jamali, 2016; Fan et al., 2018b). If the gas desorption capacity  $\rho_{wads}-P$  curve at each substantive production stage can be described linearly, the  $F_D-m(t)$  relationship can be approximated as (Crank, 1975; Etehadtavakkol and Jamali, 2016):

$$F_D = \frac{m(P_i) - m(P)}{m(P_i) - m(P_0)} = 1 - \frac{2}{R_a} \sum_{n=1}^{\infty} \frac{J_0(r \xi_n) e^{-T_0 \xi_n^2 m(t)}}{\xi_n J_1(R_a \xi_n)} \quad (15)$$

Eq. (15) is a function of both time and position. Integrating fractional production from the surface of the core to its center, the fractional production  $F_D$  for the whole core can be written as:

$$F_D = \frac{\int_0^{R_a} F_D dr}{R_a} = 1 - \frac{2}{R_a} \sum_{n=1}^{\infty} \frac{\text{hypergeom}\left(\left[\frac{1}{2}, \left[1, \frac{2}{3}\right], -1.5625 \times 10^8 \xi_n^2\right], e^{-T_0 \xi_n^2 m(t)}\right)}{\xi_n J_1(R_a \xi_n)} \quad (16)$$

where  $\text{hypergeom}(n, d, z)$  in Eq. (16) represents the generalized hypergeometric function and can be calculated using the  $\text{hypergeom}$  function in MatLab. Eq. (16) is the analytical solution of the VPG model, describing the relationship between average fractional production and pseudo-time. The pseudo-time  $m(t)$  in Eq. (16) can be estimated by Eq. (6) and the permeability and desorption rate coefficient can be estimated by a nonlinear fitting process. The nonlinear fitting process is conducted by matching the semi-analytical solution with the fractional production data obtained from dynamic gas production tests.

In order to progress the nonlinear fitting process, the semi-analytical solution of the VPG model is obtained by evaluating a sufficient number of terms needed to approximate the analytical solution. Basic petrophysical parameters used for the evaluation are shown in Table 2. Langmuir pressure  $P_L$  and Langmuir volume  $V_L$  in Table 2 are determined by fitting the Langmuir equation to shale adsorption curves (Zhang et al., 2012). Permeability and

**Table 2 Basic parameters for investigating the approximate solution of the VPG model**

Properties	Unit	Value
Sample radius, $R_a$	$\mu\text{m}$	2.5e4
Permeability, $K$	$\mu\text{m}^2$	6.2e-5
Initial gas compressibility, $c_{gi}$	1/Pa	1.11e-7
Initial gas viscosity, $\mu_i$	Pa·s	2.43e-4
Temperature, $T$	K	308.15
Initial gas pressure, $P_i$	Pa	10e6
External gas pressure, $P_0$	Pa	6e6
Skeleton density, $\rho_s$	$\text{g}/\text{cm}^3$	2.73
Langmuir pressure, $P_L$	Pa	1.315e6
Langmuir volume, $V_L$	$\text{cm}^3/\text{g}$	0.998
Desorption rate coefficient, $k_{ads}$	dimensionless	0.00665
Porosity, $\phi$	dimensionless	0.0452

desorption rate coefficients are obtained by matching the analytical solution in Eq. (16) with the first 20 terms of the infinite series with the gas dynamic production curves by using the method presented in Section 4.2.

The fitting results are presented in Fig. 4, which indicate that the first 3 terms of the infinite series in Eq. (16) are sufficient to approximate the analytical solution. Thus, the semi-analytical solution can be written as:

$$F_D = 1 - \frac{2}{R_a} \sum_{n=1}^3 \frac{\text{hypergeom}\left(\left[\frac{1}{2}, \left[1, \frac{2}{3}\right], -1.5625 \times 10^8 \xi_n^2\right] e^{-T_a \xi_n^2 m(t)}\right)}{\xi_n J_1(R_a \xi_n)} \quad (17)$$

On the basis of Eq. (17), the nonlinear fitting process can be conducted to estimate the permeability. The essence of the fitting process is an optimization problem to estimate the minima of a least-square form shown as (Yang et al., 2016):

$$\text{Min}S(\vec{P}) = \frac{1}{2} \sum_{m=1}^j (F_{Dcal}(\vec{P}, t_m) - F_{Dexp}(t_m))^2 \quad (18)$$

In Eq. (18),  $S$  is a function of the summation of squared residuals,  $\vec{P}$  is a vector containing the permeability and desorption rate coefficient,  $F_{Dcal}$  and  $F_{Dexp}$  represent the gas fractional production calculated from Eq. (17) and

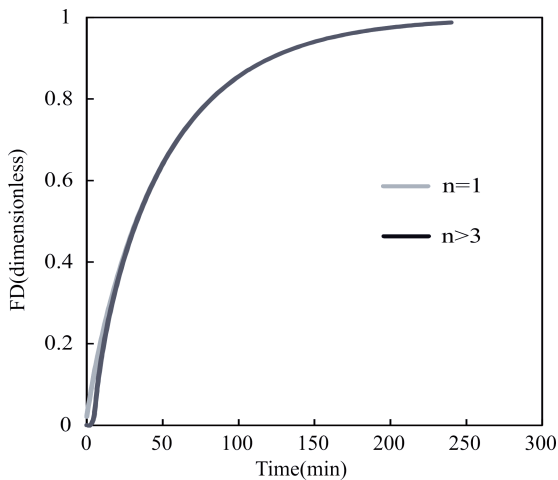


Fig. 4. Convergence test for approximating the VPG solution.

obtained from the dynamic gas production experiments, respectively,  $t_m$  is the time of the  $m^{\text{th}}$  experimental point, while  $j$  represents the total number of experimental points used for the fitting process.

The desorption rate coefficient and the permeability are estimated simultaneously using Matlab scripts. In order to avoid obtaining a local optimal result of the objective function, an iterative algorithm is applied to estimate the desorption rate coefficient and the permeability. 10,000 points are uniformly distributed for the desorption rate coefficient (from 0 to 1) together with 10,000 points for permeability (from  $1 \times 10^{-4}$  mD to  $1 \times 10^{-7}$  mD). The global optimum desorption rate coefficient and permeability are obtained by searching through this array and by storing the vector corresponding to the minimum  $\text{Min}S(K)$ .

Both average absolute error (AAE) and average absolute relative error (AARE) are used to estimate the accuracy of the calculated results, which are defined as (Feng et al., 2014; Fan et al., 2018b):

$$\text{AAE} = \frac{1}{N} \sum_{i=1}^N |F_{D,i}^{\text{exp}} - F_{D,i}^{\text{cal}}| \quad (19)$$

$$\text{AARE} = \frac{1}{N} \sum_{i=1}^N \left| \frac{F_{D,i}^{\text{exp}} - F_{D,i}^{\text{cal}}}{F_{D,i}^{\text{exp}}} \right| \quad (20)$$

where  $F_{D,i}^{\text{exp}}$  and  $F_{D,i}^{\text{cal}}$  represent the  $i^{\text{th}}$  fractional production obtained from experimental and calculated results, respectively;  $N$  represents the total amount of experimental points.

## 4 Results and Discussion

Firstly, dynamic methane production results are presented for sample #1 and sample #2. Then, a workflow for evaluation of the radial permeability is established by matching the solution of the VPG model with the experimental results. Finally, the availability and quality of the VPG method are analyzed and discussed.

### 4.1 Methane dynamic production

Figure 5 shows the results of dynamic methane production experiments on two cores under three different pressure drops at 308.15 K. It indicates that the ultimate gas accumulative production is almost the same at each gas production stage. For example, when the tests are conducted during the second stage (from approximately 6 MPa to 2 MPa), the production curves for the two cores increase gradually from the same value (around  $0.74 \text{ cm}^3/\text{g}$ ) and then equilibrate at  $1.61 \text{ cm}^3/\text{g}$ . Both the free and the adsorptive gas accumulative production are the same during a certain production stage with the same pressure gradient, which accounts for this phenomenon (Wang et al., 2016c). Figure 5 also shows that the equilibrium time for sample #1 is longer than for sample #2. i.e., the total equilibration times over the second stage are 332 min and 291 min for samples #1 and #2, respectively. The relationship between the flow direction and bedding orientation may explain this phenomenon (Wang et al., 2011). The gas flow direction is parallel to the bedding orientation for sample #2 and perpendicular to the bedding orientation for sample #1.

This indicates that the former is much more favorable for the gas flow than the latter.

#### 4.2 Parameter estimation

The gas production-time curves in Fig. 5 can be readily transformed into  $F_D-t$  for each production stage. On the basis of non-linear fitting (Matlab), the calculated results from Eq. (18) match the experimental data well as show in Fig. 6.

The estimated parameters involving permeability and desorption rate are shown in Table 3. It indicates that the

**Table 3 Results of estimated parameters**

Sample	Pressure step (MPa)	Permeability ( $10^{-6}$ mD)	Desorption rate ( $10^{-3}$ )	AAE (Dimensionless)	AARE (%)
1	9.97–5.94	8.12	8.78	0.0384	7.28
	5.94–2.04	7.94	8.13	0.0235	4.39
	2.04–0.12	7.22	7.55	0.0285	6.53
2	9.98–5.97	10.5	9.25	0.0326	8.32
	5.97–1.99	9.94	8.76	0.0107	3.56
	1.99–0.13	9.23	8.03	0.0454	8.63

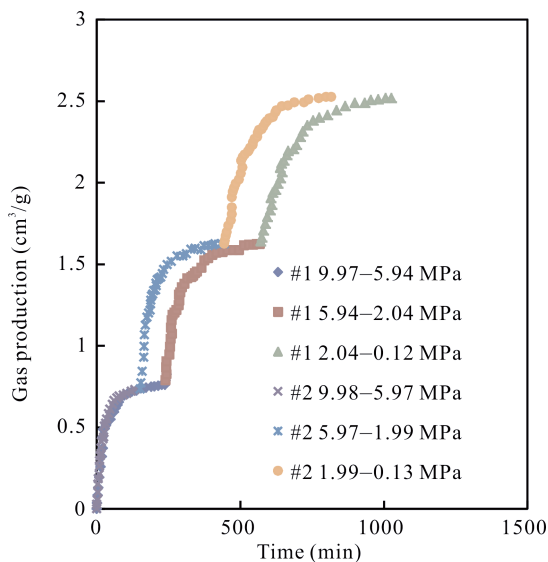


Fig. 5. Dynamic methane production results under different pressure drops for three particle sizes.

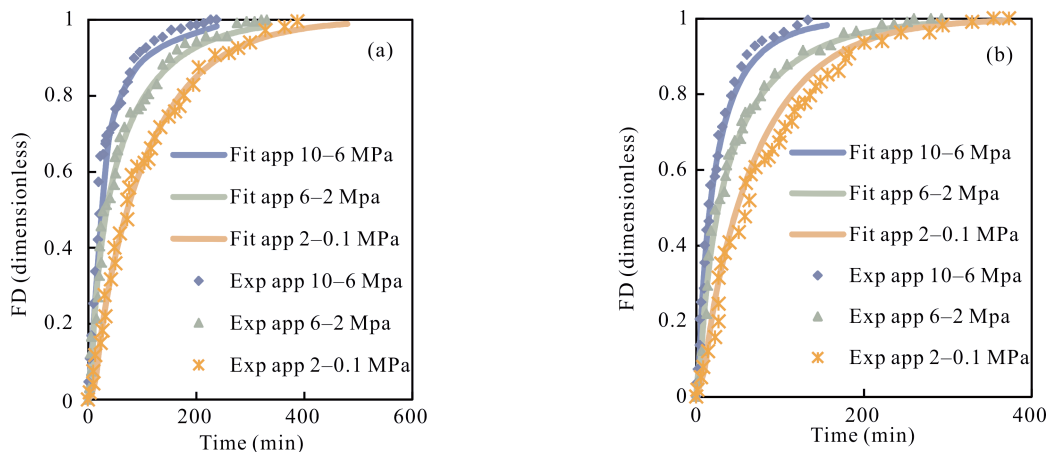


Fig. 6. FD vs. time curves for both mathematical model fits and experimental results. (a) Sample #1; (b) Sample #2.

magnitude of the gas permeability is in the range of  $1 \times 10^{-6} \text{ mD}^{-1} \times 10^{-5} \text{ mD}$ . The larger the average pore pressure, the higher the estimated permeability. Considering the experimental results of sample #1 as an example, when the boundary pressure increases from 0.12 MPa to 5.92 MPa, gas permeability increases from  $7.22 \times 10^{-6} \text{ mD}$  to  $7.94 \times 10^{-6} \text{ mD}$ . During the dynamic methane production process under a defined pressure drop, gas production contains both the free gas flow in the pore space and the progress of adsorbed gas desorption on the pore surface. The free gas flow is affected by the process of adsorbed gas desorption. Previous work (Yang et al., 2016) indicated that the gas desorption process has a delayed effect on gas recovery. Thus, when the average pressure decreases, the desorption rate decreases as shown in Table 3, leading to the observed decrease in the permeability.

Table 3 also shows that the permeability for sample #2 is larger than for sample #1 over the same pressure drop, e.g. the permeabilities are  $10.5 \times 10^{-6} \text{ mD}$  and  $8.12 \times 10^{-6} \text{ mD}$  for samples #2 and #1 within a pressure drop from approximately 10 MPa to 6 MPa, respectively. This phenomenon cannot result from changes of gas PVT properties, because the gas properties are essentially identical for the two cores within the same pressure drop. The main cause may be the difference in bedding orientation for the two samples, as discussed in the previous section. The significant permeability difference reflects the important role of bedding geometry.

#### 4.3 Model comparison and analysis

The main benefit is that the VPG model can be applied to depict gas flow under both small and large pressure drops, by using the concepts of pseudo-pressure and pseudo-time. This allows the estimated permeability from the VPG method to be directly used to depict gas flow on variable pressure gradients. When the VPG method is performed with a small pressure gradient, the pseudo-pressure in Eq. (3) and the pseudo-time in Eq. (6) can be transformed into the real pressure and time with the assumption of constant gas PVT parameters. Thus, the VPG model can be simplified into the small pressure

gradient (SPG) model (Cui et al., 2009; Cui and Abass, 2016; Yang and Dong, 2017) under the same boundary conditions. When the SPG method is applied with large pressure drops, larger errors will be obtained. As shown in Table 3 and Table 4, the average absolute error (AAE) and the average absolute relative error (AARE) of the VPG model are estimated to be in the range of 0.0107%–0.0384% and 3.56%–8.63%, respectively. The AAE and AARE of the SPG model are up to be in the range of 0.0236%–0.0632% and 6.35%–12.36%, respectively. This indicates that the VPG method has a wide range of applications than the SPG method.

Another advantage of the VPG method is that the real gas in the reservoir is used to measure permeability. An obvious derivation may exist between permeability determined using helium and using methane. Table 4 shows the results of the permeability for the two cores measured with helium by using the traditional SPG method (Cui et al., 2009). It indicates that the permeability is of the order magnitude of  $1 \times 10^{-5}$  mD, which is several times larger than the permeability estimated using methane. As discussed in the previous section, the desorption process of methane has a delayed effect on gas flow. However, the adsorption/desorption of helium in shale is negligible. Thus, values of the permeability measured with helium are larger than with methane. Table 4 also indicates that permeability decreases with an increase in the average pore pressure. This results in a smaller value of permeability at relatively high pore pressures, which is inconsistent with the permeability determined with methane. When helium flows at a relatively low pore pressure, slip flow may occur because the mean free path of the helium molecules may be of the same magnitude as the pore width (Heller et al., 2014). Conversely, the permeability for methane is smaller at relatively low pressures, because the gas flow rate is much more sensitive to decreases in the desorption process on the pore surface than increases in the slip flow in the pore space. This suggests that it is unreasonable to measure shale permeability using helium as opposed to methane.

Compared to current methods for permeability estimation, the VPG method is a straightforward method to determine permeability using real gas under variable pressure gradient conditions. However, the presented method is unable to investigate the effects of confining pressure and moisture content on the law of permeability evolution characteristics. In order to offset this shortcoming, dynamic methane production tests should be conducted on shale cores under appropriate axial

pressures, and the mathematical model should be improved to accommodate the influences of effective stresses.

## 5 Conclusions

A VPG method is established to determine shale radial permeability in cores using methane as a reservoir gas at appropriate PVT conditions and by coupling it with an appropriate model to represent dynamic gas production data. The major conclusions of this study are:

(1) The permeability of the shale measured with methane is of the magnitude of  $1 \times 10^{-6}$  mD– $1 \times 10^{-5}$  mD. Gas flow parallel to the bedding direction of the shale is much more permeable than perpendicular to the bedding orientation.

(2) Permeability obtained from the SPG method using helium is several times greater than the value obtained from methane. The real gas flow is much more sensitive to the delayed effect of the desorption process than the accelerating effect resulting from slip flow.

(3) Despite some shortcomings in the presented method, it is a useful approach to estimate shale radial permeability under representative conditions in field production.

## Nomenclature

- $\rho_s$  Skeletal density of the shale, g/cm<sup>3</sup>
- $V_{std}$  Molar volume of gas at standard temperature and pressure (i.e. 273.15K and 0.101325MPa)  $22.413 \times 10^{-3}$  m<sup>3</sup>/mol
- $V_L$  Langmuir volume, cm<sup>3</sup>/g
- $P_L$  Langmuir pressure, Pa
- $\rho$  Volume density of free gas, mol/m<sup>3</sup>
- $P$  Pressure, Pa
- $\phi_e$  Effective porosity of the shale samples, dimensionless
- $k_{ads}$  Desorption rate coefficient, dimensionless
- $r$  is the distance between the center of the radial model and the point of interest,  $\mu\text{m}$
- $\mu$  Gas viscosity, Pa·s
- $K$  Matrix permeability,  $\mu\text{m}^2$
- $t$  Time, s
- $c_g$  Gas compressibility, 1/Pa
- $Z$  Gas compressibility factor, dimensionless
- $\rho_i$  Initial gas density in void space of the shale samples, mol/m<sup>3</sup>
- $\rho_0$  Gas density in the external surface of the shale samples, mol/m<sup>3</sup>
- $P_i$  Initial gas pressure in sample chamber, Pa
- $R_a$  Radius of shale samples,  $\mu\text{m}$
- $m(P)$  Pseudo-pressure, Pa/s
- $m(t)$  Pseudo-time, s
- $\mu_i$  Gas viscosity under initial conditions, Pa·s
- $c_{gi}$  Gas compressibility under initial conditions, 1/Pa
- $Q_i$  Total gas contained in shale samples at initial pressure, cm<sup>3</sup>/g
- $V_p$  Pore volume per unit weight, cm<sup>3</sup>/g
- $Q(t)$  Accumulative gas production at actual time  $t$ , cm<sup>3</sup>/g
- $\Omega(P)$  Shale matrix production capacity at pressure  $P$ , cm<sup>3</sup>/g
- $P_0$  Gas pressure in the external surface, Pa
- $R$  Universal constant, 8.314J/(K mol)
- $T_0$  Diffusivity coefficient,  $\mu\text{m}^2/\text{s}$
- $F_D$  Fractional gas production, dimensionless
- $T$  Temperature, K

**Table 4 Results of helium permeability from the SPG method**

Sample	Pressure (MPa)	Permeability ( $10^{-5}$ mD)	AAE (Dimensionless)	AARE (%)
1	app. 10	4.12	0.0632	10.23
	app. 6	5.34	0.0326	7.53
	app. 2	6.53	0.0396	6.35
2	app. 10	5.27	0.0513	12.36
	app. 6	6.39	0.0236	6.55
	app. 2	7.98	0.0512	9.63

$T_0$  Diffusivity coefficient,  $\mu\text{m}^2/\text{s}$

$F_{Dexp,m}$  The  $m^{\text{th}}$  fractional production obtained from experiment, dimensionless

$F_{Dcal,m}$  The  $m^{\text{th}}$  fractional production obtained from the VPG model, dimensionless

$F_{Dcal}$  Calculated gas fractional production, dimensionless

$F_{Dexp}$  Experimental gas fractional production, dimensionless

$t_m$  Time corresponding to the  $m^{\text{th}}$  experimental point, s

## Acknowledgments

This paper is an enhanced version of a SPE conference presentation (SPE 191198-MS), and the full copyright of the paper has been retained by the initial owner. The authors are grateful for the important support from the 973 project (2014CB239103), the National Science, Technology Major Project (2016ZX05023-001, 2017ZX05049-006) and the Fundamental Research Funds for Central Universities (15CX06026A), the China Scholarship Council (201706450021), the National Nature Science Foundation (41772154) and the Shandong Provincial Natural Science Foundation (ZR2017MEE003).

Manuscript received Oct. 28 2019

accepted Apr. 17, 2019

associate EIC: HAO Ziguo

edited by Jeff LISTON and FEI Hongcai

## References

- Agarwal, R.G., 1979. Real gas pseudo-time—a new function for pressure buildup analysis of MHF gas wells. In: SPE Annual Technical Conference and Exhibition, 23–26 September, Las Vegas, Nevada.
- Al-Hussainy, R., Ramey, H.J., and Crawford, P.B., 1966. The flow of real gases through porous media. *Journal of Petroleum Technology*, 18: 624–636.
- API, 1998. Recommended practices for core analysis. <http://w3.energetics.org/RP40/rp40.pdf>.
- Bourbie, T., and Walls, J., 1982. Pulse decay permeability: analytical solution and experimental test. *Society of Petroleum Engineers Journal*, 22: 719–721.
- Brace, W.F., Walsh, J.B., and Frangos, W.T., 1968. Permeability of granite under high pressure. *Journal of Geophysical Research*, 73: 2225–2236.
- Brown, A.A., 2015. Interpreting Permeability from Mercury Injection Capillary Pressure Data. In: AAPG Annual Convention and Exhibition, 2 June, Denver, CO, USA.
- Bustin, R.M., Bustin, A.M.M., Cui, A., Ross, D., and Pathi, V.M., 2008. Impact of shale properties on pore structure and storage characteristics. In: SPE Shale Gas Production Conference, 16–18 November, Fort Worth, Texas, USA.
- Chen, F., Lu, S., and Ding, X., 2018. Pore types and quantitative evaluation of pore volumes in the Longmaxi Formation shale of southeast Chongqing, China. *Acta Geologica Sinica (English Edition)*, 92(1): 342–353.
- Chen, S.B., Zhu, Y.M., Wang, H.Y., Liu, H.L., Wei, W., and Fang, J.H., 2011. Shale gas reservoir characterisation: A typical case in the southern Sichuan Basin of China. *Energy*, 36(11): 6609–6616.
- Cicha-Szot, R., Dudek, L., and Such, P., 2015. Permeability estimation in shale formations on the basis of desorption data and radial gas flow model. *Nafta-Gaz*, 71: 833–839.
- Crank, J., 1975. *The Mathematics of diffusion*, second ed, Clarendon Press, New York.
- Cui, Q., and Abass, H.H., 2016. Experimental Study of Permeability Decline in Tight Formations During Long-Term Depletion. In: SPE Low Perm Symposium, 5–6 May, Denver, Colorado, USA.
- Cui, X., and Bustin, A.M.M., Bustin, R.M., 2009. Measurements of gas permeability and diffusivity of tight reservoir rocks: different approaches and their applications. *Geofluids*, 9: 208–223.
- Daigle, H., and Dugan, B., 2011. An improved technique for computing permeability from NMR measurements in mudstones. *Journal of Geophysical Research: Solid Earth*, 116: 1–14.
- Ettehadtavakkol, A., and Jamali, A., 2016. Measurement of shale matrix permeability and adsorption with canister desorption test. *Transport in Porous Media*, 114: 149–167.
- Fan, C., Li, S., Luo, M., Du, W., and Yang, Z., 2017. Coal and gas outburst dynamic system. *International Journal of Mining Science and Technology*, 27: 49–55.
- Fan, C., Li, S., Luo, M., Yang, Z., and Lan, T., 2018a. Numerical simulation of hydraulic fracturing in coal seam for enhancing underground gas drainage. *Energy Exploration & Exploitation*, 37(1): 166–193.
- Fan, C.H., Zhong, C., Zhang, Y., Qin, Q.R., and He, S., 2019. Geological factors controlling the accumulation and high yield of marine-facies shale gas: case study of the Wufeng-Longmaxi Formation in the Dingshan area of Southeast Sichuan, China. *Acta Geologica Sinica (English Edition)*, 93(3): 536–560.
- Fan, K., Dong, M., Elsworth, D., Li, Y., Yin, C., and Li, Y., 2018b. A dynamic-pulse pseudo-pressure method to determine shale matrix permeability at representative reservoir conditions. *International Journal of Coal Geology*, 193: 61–72.
- Feng, Q., Zhang, J., Zhang, X., Shu, C., Wen, S., Wang, S., and Li, J., 2014. The use of alternating conditional expectation to predict methane sorption capacity on coal. *International Journal of Coal Geology*, 121: 137–147.
- Freeman, C.M., Moridis, G.J., and Blasingame, T.A., 2011. A Numerical Study of Microscale Flow Behavior in Tight Gas and Shale Gas Reservoir Systems. *Transport in Porous Media*, 90: 253–268.
- Guo, C., Wei, M., and Liu, H., 2018. Study of gas production from shale reservoirs with multi-stage hydraulic fracturing horizontal well considering multiple transport mechanisms. *Plos One*, 13: 1–21.
- Guo, C., Xu, J., Wu, K., Wei, M., and Liu, S., 2015. Study on gas flow through nano pores of shale gas reservoirs. *Fuel*, 143: 107–117.
- Guo, W., Hu, Z., Zhang, X., Yu, R., and Wang, L., 2017. Shale gas adsorption and desorption characteristics and its effects on shale permeability. *Energy Exploration & Exploitation*, 35: 463–481.
- Guo, X., Hu, D. F., Li, Y. P., Liu, R., and Wang, Q., 2014a. Geological features and reservoiring mode of shale gas reservoirs in Longmaxi Formation of the Jiaoshiba area. *Acta Geologica Sinica (English Edition)*, 88(6): 1811–1821.
- Guo, X., Li, Y., Liu, R., and Wang, Q., 2014b. Characteristics and controlling factors of micro-pore structures of Longmaxi Shale Play in the Jiaoshiba area, Sichuan Basin. *Natural Gas Industry*, 34: 9–16.
- Haskett, S.E., Narahara, G.M., and Holditch, S.A., 1988. A method for simultaneous determination of permeability and porosity in low-permeability cores. *SPE Formation Evaluation*, 3: 651–658.
- Heller, R., Vermynen, J., and Zoback, M., 2014. Experimental investigation of matrix permeability of gas shales. *AAPG Bulletin*, 98: 975–995.
- Hsieh, P.A., Tracy, J.V., Neuzil, C.E., Bredehoeft, J.D., and Silliman, S.E., 1981. A transient laboratory method for determining the hydraulic properties of “tight” rocks-I. Theory. *International Journal of Rock Mechanics and Mining Sciences & Geomechanics Abstracts*, 18: 245–252.
- Huang, C., Xu, T.Y., Ju, Y.W., Zhu, H.J., Ju, L.T., and Li, W.Y., 2019. Fracability evaluation of shale of the Wufeng-Longmaxi. *Acta Geologica Sinica (English Edition)*, 93(4): 996–1004.
- Formation in the Changning Area, Sichuan Basin
- Javadpour, F., 2009. Nanopores and apparent permeability of gas

- flow in mudrocks (shales and siltstone). *Journal of Canadian Petroleum Technology*, 48: 16–21.
- Javadpour, F., Fisher, D., and Unsworth, M., 2007. Nanoscale gas flow in shale gas sediments. *Journal of Canadian Petroleum Technology*, 46: 55–61.
- Jones, S.C., 1997. A Technique for faster pulse-decay permeability measurements in tight rocks. *SPE Formation Evaluation*, 12: 19–26.
- Jones, S.C., 1972. A rapid accurate unsteady-state Klinkenberg permeameter. *Society of Petroleum Engineers Journal*, 12: 383–397.
- Knabe, R., and Wang, Y., 2011. Permeability characterization on tight gas samples using pore pressure oscillation method. *Petrophysics*, 52: 437–443.
- Li, Z., Wang, S., Li, S., Liu, W., Li, B., and Lv, Q.C., 2014. Accurate determination of the CO<sub>2</sub>-brine interfacial tension using graphical alternating conditional expectation. *Energy & Fuels*, 28: 624–635.
- Lin W., 2016. A review on shale reservoirs as an unconventional play – the history, technology revolution, importance to oil and gas industry, and the development future. *Acta Geologica Sinica (English Edition)*, 90(5): 1887–1902.
- Liu, X., 2016. Well test analysis and evaluation after shale-gas volume fracturing stimulation. *Natural Gas Industry*, 36: 66–72.
- Luffel, D.L., Hopkins, C.W., and Schettler, P.D., 1993. Matrix permeability measurement of gas productive shales. In: *SPE Annual Technical Conference and Exhibition*, 3–6 October, Houston, Texas, USA.
- Luo, J., Dai, H., Shao, L., Wang, W., and Li, N., 2012. Prospect prediction for shale gas resources of the Lower Paleozoic in Sichuan Basin. *Lithologic Reservoirs*, 24(4): 71–74 (in Chinese with English abstract).
- Neuzil, C.E., Cooley, C., Silliman, S.E., Bredehoeft, J.D., and Hsieh, P.A., 1981. A transient laboratory method for determining the hydraulic properties of “tight” rocks-II. Application. *International journal of rock mechanics and mining sciences & geomechanics abstracts*, 18: 253–258.
- Nie, H., and Jin, Z., 2016. Source rock and cap rock controls on the Upper Ordovician Wufeng Formation–Lower Silurian Longmaxi Formation shale gas accumulation in the Sichuan Basin and its peripheral areas. *Acta Geologica Sinica (English Edition)*, 3: 1059–1060.
- Okamoto, N., Liang, Y., Murata, S., Matsuoka, T., Akai, T., and Takagi, S., 2015. Slip velocity and permeability of gas flow in nanopores for shale gas. In: *SPE Asia Pacific Unconventional Resources Conference and Exhibition*, 9–11 November, Brisbane, Australia.
- Ou, C., and Li, C., 2017. 3D discrete network modeling of shale bedding fractures based on lithofacies characterization. *Petroleum Exploration and Development*, 44: 336–345.
- Ozkan, E., Raghavan, R.S., and Apaydin, O.G., 2010. Modeling of fluid transfer from shale matrix to fracture network. In: *SPE Annual Technical Conference and Exhibition*, 19–22 September, Florence, Italy.
- Parvizi, H., Rezaei Gomari, S., Nabhani, F., and Dehghan Monfared, A., 2018. Modeling the risk of commercial failure for hydraulic fracturing projects due to reservoir heterogeneity. *Energies*, 11: 218.
- Qu, H., Zhou, F., Xue, Y., and Key, S., Resources, P., 2015. Experimental study of controlling factors of the continental shale matrix permeability in Ordos Basin geologic characterization of the Yanchang Formation 1–13. In: *SPE Asia Pacific Unconventional Resources Conference and Exhibition*, 9–11 November, Brisbane, Australia.
- Rahman, N.M.A., Mattar, L., and Zaoral, K., 2004. A new method for computing pseudo-time for real gas flow using the material balance equation. *Journal of Canadian Petroleum Technology*, 10: 36–44.
- Ran, B., Liu, S., Jansa, L., Sun, W., Yang, D., Wang, S., and Luo, C., 2016. Reservoir characteristics and preservation conditions of longmaxi shale in the Upper Yangtze block, South China. *Acta Geologica Sinica (English Edition)*, 90(6): 2182–2205.
- Revil, A., and Florsch, N., 2010. Determination of permeability from spectral induced polarization in granular media. *Geophysical Journal International*, 181: 1480–1498.
- Ross, D.J.K., and Bustin, R.M., 2007. Shale gas potential of the Lower Jurassic Gordondale Member, northeastern British Columbia, Canada. *Bull. Bulletin of Canadian Petroleum Geology*, 55: 51–75.
- Shan, Q., Jin, Y., Tan, P., and Zhang, R., 2018. Experimental and numerical investigations on the vertical propagation of hydraulic fractures in laminated shales. *Journal of Geophysics and Engineering*, 15(4): 1729–1742.
- Sinha, S., Braun, E.M., Passey, Q.R., Leonardi, S.A., Wood III, A.C., Zirkle, T., Boros, J.A., and Kudva, R.A., 2012. Advances in Measurement Standards and Flow Properties Measurements for Tight Rocks such as Shales. In: *SPE/EAGE European Unconventional Resources Conference and Exhibition*, 20–22 March, Vienna, Austria.
- Song, Y., Jiang, B., and Qu, M., 2018. Molecular Dynamic Simulation of Self- and Transport Diffusion for CO<sub>2</sub>/CH<sub>4</sub>/N<sub>2</sub> in Low-Rank Coal Vitrinite. *Energy & Fuels*, 32: 3085–3096.
- Suarez-Rivera, R., Chertov, M., Willberg, D., Green, S., and Keller, J., 2012. Understanding Permeability Measurements in Tight Shales Promotes Enhanced Determination of Reservoir Quality. In: *SPE Canadian Unconventional Resources Conference*, 30 October–1 November, Calgary, Alberta, Canada.
- Tian, S., Ren, W., Li, G., Yang, R., and Wang, T., 2017. A Theoretical Analysis of Pore Size Distribution Effects on Shale Apparent Permeability. *Geofluids*, 2017: 1–9.
- Tong, M., Li, L., Wang, W., and Jiang, Y., 2006. A time-domain induced-polarization method for estimating permeability in a shaly sand reservoir. *Geophysical Prospecting*, 54: 623–631.
- Wang, C., Liu, J., Feng, J., Wei, M., Wang, C., and Jiang, Y., 2016a. Effects of gas diffusion from fractures to coal matrix on the evolution of coal strains: Experimental observations. *International Journal of Coal Geology*, 162: 74–84.
- Wang, C., Zhai, P., Chen, Z., Liu, J., Wang, L., and Xie, J., 2017a. Experimental study of coal matrix-cleat interaction under constant volume boundary condition. *International Journal of Coal Geology*, 181: 124–132.
- Wang, J., Wang, B., Li, Y., Yang, Z., Gong, H., and Dong, M., 2016b. Measurement of dynamic adsorption–diffusion process of methane in shale. *Fuel*, 172: 37–48.
- Wang, J., Yang, Z., Dong, M., Gong, H., Sang, Q., and Li, Y., 2016c. Experimental and numerical investigation of dynamic gas adsorption/desorption–diffusion process in shale. *Energy & Fuels*, 30: 10080–10091.
- Wang, S., Elsworth, D., and Liu, J., 2011. Permeability evolution in fractured coal: The roles of fracture geometry and water-content. *International Journal of Coal Geology*, 87: 13–25.
- Wang, Y., Cheng, S., Feng, N., He, Y., and Yu, H., 2017b. The physical process and pressure-transient analysis considering fractures excessive extension in water injection wells. *Journal of Petroleum Science and Engineering*, 151: 439–454.
- Wu, X., Liu, Q., Liu, G., Wang, P., Li, H., Meng, Q., and Zeng, H., 2017. Geochemical characteristics and genetic types of natural gas in the Xinchang Gas Field, Sichuan Basin, SW China. *Acta Geologica Sinica (English Edition)*, 91(6): 2200–2213.
- Yang, Z., and Dong, M., 2017. A new measurement method for radial permeability and porosity of shale. *Petroleum Research*, 2: 178–185.
- Yang, Z., Sang, Q., Dong, M., Zhang, S., Li, Y., and Gong, H., 2015. A modified pressure-pulse decay method for determining permeabilities of tight reservoir cores. *Journal of Natural Gas Science and Engineering*, 27: 236–246.
- Yang, Z., Wang, W., Dong, M., Wang, J., Li, Y., Gong, H., and Sang, Q., 2016. A model of dynamic adsorption–diffusion for modeling gas transport and storage in shale. *Fuel*, 173: 115–128.
- Yu, M., Weinthal, E., Patiño-Echeverri, D., Deshusses, M.A., Zou, C., Ni, Y., and Vengosh, A., 2016. Water availability for shale gas development in Sichuan Basin, China. *Environmental Science & Technology*, 50(6): 2837–2845.

- Yuan, W., Pan, Z., Li, X., Yang, Y., Zhao, C., Connell, L.D., Li, S., and He, J., 2014. Experimental study and modelling of methane adsorption and diffusion in shale. *Fuel*, 117: 509–519.
- Zhang, M., and Ayala, L., 2015. Density-based production-data analysis of gas wells with significant rock-compressibility effects. *SPE Reservoir Evaluation & Engineering*, 18: 205–213.
- Zhang, Z., and Yang, S., 2012. Study on the adsorption and desorption trend of shale gas. *Journal of Experimental Mechanics*, 27(4): 492–497 (in Chinese with English abstract).
- Zhao, J., Jin, Z., Jin, Z., Wen, X., and Geng, Y., 2016. Physical mechanism of organic matter - mineral interaction in Longmaxi Shale, Sichuan Basin, China. *Acta Geologica*

*Sinica* (English Edition), 90(5): 1923–1924.

#### **About the first and corresponding author**



FAN Kunkun, male, born in Zibo City, Shandong Province; doctor; graduated from the Chinese University of Petroleum (East China); lecturer of the College of Energy and Mining Engineering, Shandong University of Science and Technology. He is currently interested in research on the theory and application of unconventional oil and gas seepage and geothermal energy development. Email: fankunkun06@qq.com; phone: 86-17660233272.